

Fabrication Processes of MEMS Phase Shifters on Polymer-based Substrates

Jianqun Wang, Thermpoon Ativanichayaphong, Ying Cai, Wen-Ding Huang,
Lun-Chen Hsu, W. Alan Davis, Mu Chiao* and J.-C. Chiao

Department of Electrical Engineering, University of Texas at Arlington, TX 76019

* Department of Mechanical Engineering, University of British Columbia, Canada

ABSTRACT

RF phase shifters find wide applications in telecommunications, satellite systems, personal wireless communication systems, radar systems, tracking systems, and sensors. They have been conventionally manufactured by semiconductor technologies which suffer from high insertion losses due to high RF series resistances. They are expensive due to fabrication and assembly costs.

The RF MEMS phase shifters provide low insertion losses, low fabrication costs and high linearity compared with the semiconductor ones. Furthermore, polymer materials have demonstrated low material costs and low RF attenuations. In this work, we proposed to build RF MEMS phase shifters on polymer substrates. The proposed devices were successfully manufactured and tested from DC to 26 GHz. Our experimental results indicated more than 35 degrees phase shifts and low insertion losses.

INTRODUCTION

Polymers present many advantages over traditional semiconductor materials. The low RF attenuations [1-3], low dielectric constants and high resistivities [4,5] make them popular choices for high quality-factor RF applications. The low curing temperatures, high planarization degree, high thermal stability and superb chemical resistances are ideally suited for existing IC fabrication technologies. The polymers provide for versatile micromachining abilities. 3-D structures can be made by plasma etching [6], deep reactive ion etching, photolithography or hot embossing techniques. In recent years, research has been conducted in the fields of the micro-fluidic devices, wafer bonding and polymer-silicon integration [7-9]. However, polymers in RF applications are not fully explored yet.

As the core component of many modern communication systems, most phase shifters are currently based on semiconductor or ferrites devices [10]. High material and fabrication expenses, as well as the high RF losses associated with the materials, are drawbacks which hinder their further applications. RF MEMS uses conductive materials, such as metals, to form mechanically-deformable structures that can alter wave propagation characteristics. For example, the RF MEMS approach of a true-time delay utilizes a series of MEMS bridge varactors over a coplanar waveguide (CPW) transmission line. Electrostatic forces generated by applying voltages across the MEMS bridges reduce bridge heights and increase loaded capacitances. The variable capacitances change phase velocities and create phase shifting. Many RF MEMS phase shifters and related applications have been demonstrated on quartz [11], high resistivity silicon [10,12], and III-V compound substrates [13]. These showed great results such as provide lower attenuations, consume less power, and present higher linearity than semiconductor components.

Owing to the unique properties of polymers and the excellent performances of the RF MEMS device architectures, we present RF phase shifters built on polymer substrates. In this work, we investigated the design considerations, fabrication processes and experimental results of the RF MEMS phase shifters on polymer substrates.

DESIGN CONSIDERATIONS

The uniplanar attribute of coplanar waveguide transmission lines enables construction of all the components on the same side of the substrates. This unique feature reduces manufacture steps, allows using on-wafer characterization techniques [14] and creates less expensive fabrication processes. CPW transmission lines are widely utilized as interconnects in microwave integrated circuits. They are also the essential building blocks of the RF MEMS phase shifters, impedance tuners and switches.

To minimize the losses, the characteristic impedance Z_o of the CPW transmission line needs to match that of the rest of the circuitry. For most of the RF applications, the characteristic impedance is 50 Ω . The characteristic impedance of an unloaded CPW transmission line, without loading MEMS bridges, is a function of the CPW physical dimension, as well as of the dielectric properties of the substrate materials. In our work, polyimide ($\epsilon_r=3.5$) and benzocyclobutene (BCB, $\epsilon_r=2.65$) polymers were chosen to be the dielectric layers due to their low insertion losses, low material costs and the ease of processing them [1-3].

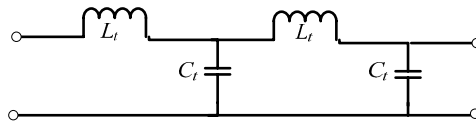


Figure 1. The unit-length equivalent circuit of an unloaded CPW line.

Fig. 1 shows the unit-length equivalent circuit of an unloaded CPW transmission line, where L_t and C_t are the unit-length inductance and capacitance, respectively. The relationship between L_t , C_t and the unloaded characteristic impedance Z_o is [15,11],

$$L_t = C_t Z_o^2 \text{ and } C_t = \frac{\sqrt{\epsilon_{eff}}}{c Z_o} \quad (1)$$

where the ϵ_{eff} is the effective dielectric constant, and c is the speed of light in vacuum. The phase velocity V_t of the unloaded CPW transmission lines is [15]

$$V_t = \frac{1}{\sqrt{L_t C_t}} \quad (2)$$

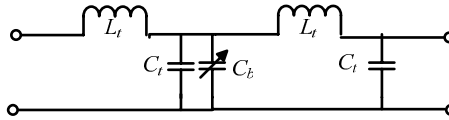


Figure 2. The unit-length equivalent circuit of a loaded CPW line.

Loading a CPW transmission line with periodic MEMS bridges adds shunt capacitances C_b in parallel to the C_t . The modified unit equivalent circuit is shown in Fig. 2. The total capacitance of the loaded CPW transmission line thus becomes $C_t = C_b/s + C_t$, where s is the periodic spacing between two adjacent MEMS bridges. The increased capacitance slows down the phase velocity and thus creates phase shifting. The loaded CPW line phase velocity is given by *Barker* [11]

$$V_l = \frac{1}{\sqrt{L_t (C_t + C_b / s)}} \quad (3)$$

Placing MEMS bridges over a CPW transmission line decreases the characteristic impedance as well. Eq. (4) gives the loaded characteristic impedance [11]. To obtain a minimum transmission loss, the dimensions of the CPW transmission lines need to be properly designed so that the loaded characteristic impedance can be close to 50 Ω .

$$Z_l = \sqrt{\frac{L_t}{C_t + C_b / s}} \quad (4)$$

$$C_b = \epsilon_{eff} \frac{A}{d} \text{ and } A = W \times w \quad (5)$$

The capacitance of each MEMS bridge is governed by Eq. (5), where A is the MEMS bridge area determined by the width of the CPW center conductor line (W) and the bridge width (w), d is the height between the MEMS bridges and the CPW center conductor line. Applying voltages across MEMS bridges generates electrostatic forces pulling the MEMS bridges toward the CPW center conductor line and increases the MEMS bridge capacitance C_b .

However, the CPW line with periodically distributed bridges has an upper operational frequency limit at which the guided wavelength is comparable to the spacing of bridges. Beyond this frequency, the CPW transmission line becomes reactive and return loss increases. This frequency is called Bragg frequency and is given by [11, 16].

$$f_{Bragg} = \frac{1}{\pi s \sqrt{L_i (C_i + C_b / s)}} \quad (6)$$

This indicates, with loaded MEMS bridges, that the Bragg frequency was lower than the unloaded one.

Taken all the above elements and convenience for probing into consideration, the CPW line dimensions were chosen to have a spacing (S) and a signal-line width (W) of 100- μm , similar to *Barker's* design. The CPW transmission line of such dimensions has an unloaded characteristic impedance greater than 100 Ω with either polyimide or BCB as the dielectric layer and glass as the substrate. The bridge spacing (s) also impacts the phase shifting values. It not only determines the traveling distance of guided waves, but also the per unit-length loaded capacitance. Bridge spacings of 300, 400, 500 and 600- μm were chosen for design comparison. The bridge width (w) plays a significant role in two parameters: it affects the loaded capacitance, namely phase shifting, and the transmission loss. After careful consideration, the bridge widths of 30- and 60- μm were selected.

The devices were measured with GSG (ground-signal-ground) probes which have dimensions of 150- μm spacing and 50- μm width. The CPW line has dimensions of 100- μm spacing and 100- μm width. A taper type of impedance transition was designed not only to accommodate the dimensional difference, but also to avoid an abrupt impedance change between the CPW line and the feeding pads [3,17].

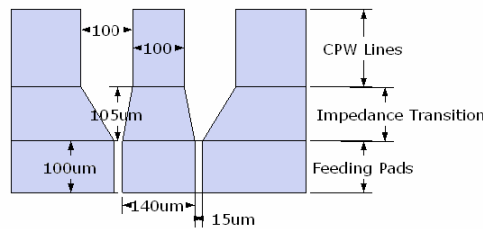


Figure 3. The taper impedance transition.

The actuation voltage is given by Eq (7), where V_{bias} is the actuating voltage across the MEMS bridges, and ϵ_o is the free space permittivity. Only one third of the bridge height (d) can be used to change the MEMS capacitance due to the capacitive MEMS pull-in condition [11]. Beyond one third of the bridge height, the MEMS bridges will collapse onto the CPW center conductor line. The voltage at which this collapse happens is called the “pull-in voltage” given by Eq. (8),

$$F = \frac{\epsilon_o W w}{2d^2} V_{bias}^2 \quad (N) \quad (7)$$

$$V_p = \sqrt{\frac{8k}{27\epsilon_o W w}} d_o^3 \quad (V) \quad (8)$$

where k is the spring constant of the bridge membrane as a function of its dimensions, material strength, and surface stress level [11].

FABRICATION PROCESS

(a) Polymer Deposition

Glass substrates were cleaned with an acetone ultrasonic bath for 2 minutes to remove surface contaminations and followed by 1-minute hotplate baking at 100°C to dehydrate any residual liquid on glass surfaces. Two types of polymers were selected as the dielectric materials: benzocyclobutene (BCB) and polyimide. For BCB polymer deposition, the surface promoter AP3000 was applied by spin-on process at 3000 rpm for 20 seconds, followed by hotplate baking at 100°C for 1 minute. BCB resin was spun on at 2000 rpm for 30 seconds, which gave more than a 10- μm thickness. A heating process was performed at 90°C for 1 minute to obtain a firmer polymer layer and to avoid polymer reflowing during the curing process. For polyimide deposition, the same process steps were performed except no surface promoter was needed. The polyimide has a very good self-adhesive property [5].

The hard curing step for BCB was conducted inside a nitrogen-purged environment oven ramping slowly from the room temperature to 250°C at which the curing process lasted for one hour. Such a heating step cures more than 95% of the polymer [4]. The curing temperature for the polyimide was 350°C, the rest of curing profile was the same as that of BCB. Fig. 4 (a) shows a polymer layer on a glass substrate.

(b) CPW Metal Formation

Samples were washed with acetone in an ultrasonic bath to remove any cross contaminations. NR7 negative photoresist was spun on top of the polymers at 3000 rpm for 40 seconds, followed by 150°C hotplate baking for 1 minute. Next, the CPW patterns were exposed through a soda lime photomask. Post exposure bake (PEB) was performed at 100°C for 1 minute. The samples were then developed in RD6 developer with agitation for 25-30 seconds, followed by a DI water rinse and nitrogen air drying.

A sandwich metal layer of chromium-aluminum-chromium was deposited using the thermal evaporation technique. The thickness of the Cr-Al-Cr layers is 500-8000-500 Å, respectively. The two Cr layers functioned as adhesion materials. Our experiments showed that without adhesion metals, the aluminum CPW layer neither stayed on the polymer sturdily nor stuck to the MEMS bridges firmly in the later processing steps.

The samples were soaked in acetone solvent overnight for metal liftoff. Most of unexposed negative photoresist NR7-3000p together with the metals on top of it were lifted off by acetone soaking and a short time ultrasonic agitation (less than 2 minutes). However, due to the uncertainty of the photolithography and excessive thermal evaporation heating, the NR7 may be partially overexposed and cured. Thus it was not easy to be lifted off by the acetone soak and ultrasonic bath completely. In this case, 10 minutes of RR2 hot bath (80°C) would be adequate to give a clean liftoff. Fig. 4 (b) shows the cross section of a CPW transmission line on the polymer-glass substrate.

(c) Silicon Nitride Growth

The samples were cleaned with an acetone wash. Ultrasonic process was avoided in this step, because the metal layer formed in the last step was vulnerable to the ultrasonic waves. The patterns of the CPW center conductor insulating layer were defined by the same photolithography processes. A silicon nitride insulating layer of 3000 Å was grown using a RF sputtering technique. A lift-off process again was performed with the same conditions as in the previous step. Fig. 4 (c) shows the silicon nitride on the CPW center conductor.

(d) Sacrificial Layer Deposition

The samples were washed with acetone before the positive photoresist S1813 was used to form the sacrificial layer. The S1813 was spun on the samples at 2500 rpm for 30 seconds, followed by hotplate baking at 105°C for 70 seconds. Such spinning speed gave about a 1.75 μm thick photoresist layer. The photoresist layer was

patterned with the sacrificial photomask by the photolithography. The samples were developed for 30 seconds in MF319 developer. The samples were then heated on a hotplate at 130°C for 3.5 minutes. This post-developing bake was critical. It would give the sacrificial layer enough robustness, yet the photoresist would still be able to be dissolved later by the photoresist stripper. A different heating profile may either cure the photoresist or would not generate a firm sacrificial layer. Fig. 4 (d) shows the sacrificial layer.

(e) Bridge Formation

A copper layer of 1.5- μm thickness was deposited using a thermal evaporation process. During the evaporation, samples were rotated at different angles to ensure an evenly grown copper layer. Bridges patterns were defined using a photoresist S1813 layer by the photolithography process. The photoresist served as a mask for copper etching. The etching process was performed in APS100 copper etchant at 50°C for 30 seconds. Fig. 4 (e) illustrates this bridge formation process.

(f) Device Release

The samples were soaked inside an 1165 photoresist stripper overnight, followed by alcohol rinsing with agitation. To avoid the bridge stiction, the samples were baked at 110°C for 10 minutes to quickly evaporate the alcohol residues. Fig. 4 (f) shows a bridge after releasing and (g) shows a 3-D sketch of a phase shifter.

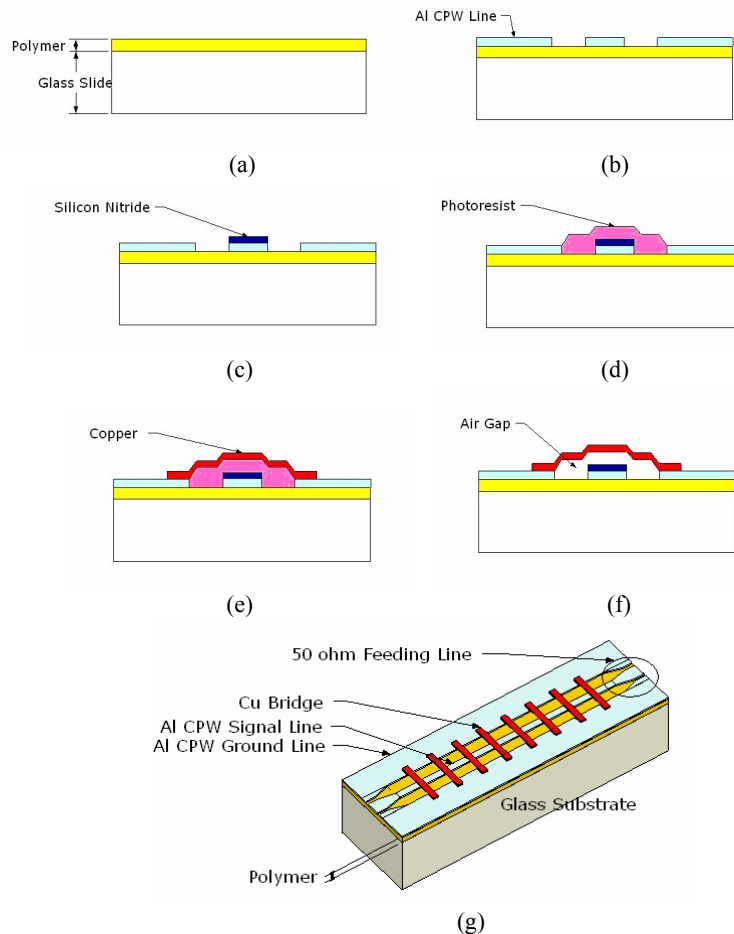


Figure 4. Fabrication processes. (a) Polymer deposition. (b) CPW transmission line formation. (c) Silicon nitride growth. (d) Sacrificial layer deposition. (e) Bridge formation. (f) Device release. (g) A 3-D sketch of a phase shifter.

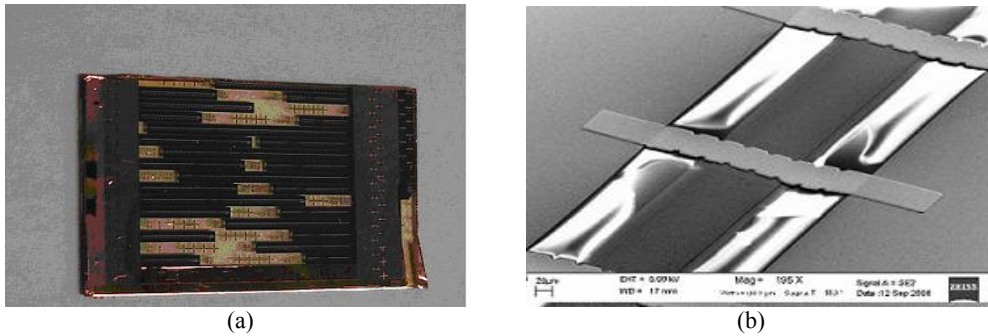


Figure 5. (a) A photo of phase shifters on the polymer dielectric layer and glass substrate. (b) A SEM photo of MEMS bridges over a CPW center conductor line.

EXPERIMENTAL RESULTS

The RF MEMS phase shifters on polymer-glass based substrates were successfully manufactured. The devices were characterized with an *Agilent 8510* network analyzer and two *Cascade Microtech Infinity GSG-150* probes from DC to 26 GHz. The scattering parameter measurements were calibrated by the *Cascade Microtech ISS-005-016* impedance standard substrates. The DC actuating voltages were applied by a HP4142B DC source and a HP 11612 biasing network.

Fig. 5 (a) shows a photo of phase shifters on the polymer dielectric layer and glass substrate; Fig. 5 (b) shows a scanning electron microscopic (SEM) picture of MEMS bridges over a CPW center conductor line. The bridge has dimensions of 60- μm width and 300- μm length. The entire phase shifter length is 6.5-mm. Our measurement results indicate that, with 16 MEMS bridges, a bridge spacing of 300- μm , a bridge width of 60- μm , and a BCB dielectric layer of 10- μm , the phase shift reaches 35° linearly as the frequency increases. Fig. 6 (a) shows with biasing voltages of 10V, 20V and 25V, the phase shifts are 7°, 25° and 35° at 26 GHz, respectively. The phase shifts are 5°, 14° and 18° at 15GHz. Fig. 6 (b) shows the insertion and return losses. The insertion losses were consistently found to be 2.5 dB at 26 GHz regardless of the different biasing voltages.

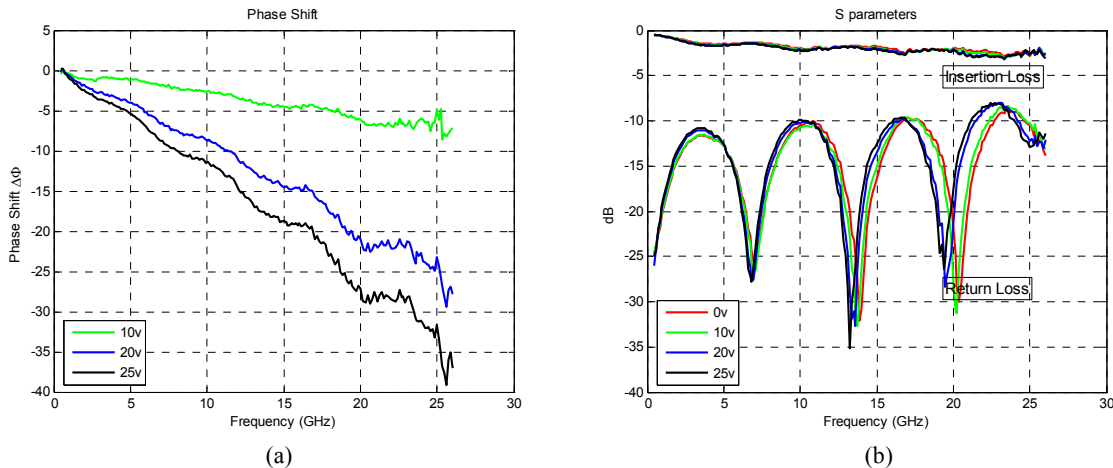


Figure 6. Experimental results of a phase shifter. (a) Phase shifts with different biasing voltages. (b) Insertion and return losses.

To verify the experimental results, the insertion loss and return loss were simulated using the finite element method (FEM). The simulation results agree well with the experimental measurements. The simulated insertion loss of 2 dB (Fig. 7) is slightly lower than that of experimental results (2.5 dB). The reason for this discrepancy was most likely due to the idealized assumptions such as the zero loss tangent and zero

conductivity of BCB in the simulation configuration. Also, the fabrication process may be subject to some uncertain variations.

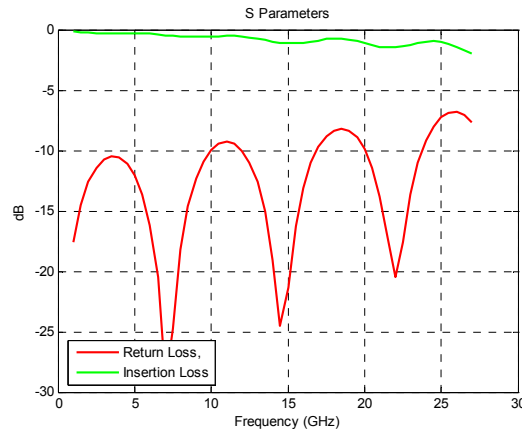


Figure 7. Simulation results of a RF MEMS phase shifter.

CONCLUSIONS

In this paper, we investigated the design, fabrication techniques and performance of RF phase shifters on polymer substrates. Our measurement indicates that the phase shift reaches 35° at 26 GHz. The insertion loss is about 2.5 dB. The fabrication processes used low cost materials and gave repeatable results.

ACKNOWLEDGEMENT

This research is sponsored by the National Science Foundation DMI #0428884.

The authors would like to express their gratitude to Dr. N. Scott Barker for his help and valuable suggestions on fabrication, Dr. Ronald Carter for his help on characterization supports, and Dr. Nasir Basit and Mr. Dennis Bueno for their cleanroom assistance.

REFERENCE

1. K. Grenier, V. Lubecke, F. Bouchriha, L. Rabbia, D. Dubuc, P. Pons, and R. Plana, "Polymer in RF and millimeterwave applications," *Proc. of SPIE*, Volume 5116, pp. 502-513, 2003.
2. L.L.W. Leung, Wai-Cheong Hon and K. J. Chen, "Low-loss coplanar waveguides interconnects on low-resistivity silicon substrate," *IEEE Transactions Components and Packaging Technologies*, Volume 27, Issue 3, pp.507 - 512, Sept. 2004.
3. Jianqun Wang, Ying Cai, Thermpoon Ativanichayaphong, Mu Chiao and J.-C. Chiao, "Fabrication techniques and RF performances of transmission lines on polymer substrates," *Proc. of SPIE*, Volume 6035, 2006.
4. *DOW Processing Procedures For CYCLOTENE™ 4000 Series Resin.*
5. *HD MicroSystems PI-2730 Series Low Stress Photodefinable Polyimide Product Information and Process Guidelines.*
6. Sang Won Park, Kabseog Kim, Jeong-Bong Lee, and Wendel Alan Davis, "Plastic-based pattern transfer process for RF MEMS passives," *IEEE 2002 Emerging Telecommunication Technologies Conference*, Richardson, TX, September 2002.

7. D. O. Popa, et. al., "BCB wafer bonding for microfluidics", *TEXMEMS VI Conference*, Texas A&M, September 2004.
8. N. Ghalichechian, A. Modafe, R. Ghodssi, P. Lazzeri, R. Micheli, and M. Anderle, "Integration of benzocyclobutene polymers and silicon micromachined structures using anisotropic wet etching," *Journal of Vacuum Science and Technology B: Microelectronics and Nanometer Structures*, vol.22, pp. 2439-2447, September 2004.
9. D. O. Popa, T.J. Hwang, J.Q. Lu, B.H. Kang, and H. Stephanou, "BCB Wafer Bonding Compatible with Bulk Micro machining", in *Proc. of Int'l Electronic Packaging Technical Conference and Exhibition*, INTERPACK '03, Maui, Hawaii, July 2003.
10. T.S. Ji, K.J. Vinoy, and V.K. Varadan, "Distributed MEMS phase shifters by microstereolithography on silicon substrates for microwave and millimeter wave applications," *Smart Materials and Structures*, vol. 10, pp. 1224-1229, 2001.
11. N. S. Barker and G. M. Rebeiz, "Distributed MEMS true-time delay phase shifters and wide band switches," *IEEE Trans. Microwave Theory Tech.*, vol. 46, Issue 11, pp. 1881-1890, Nov. 1998.
12. Jian Qing, Yanling Shi, Wei Li, Zongsheng Lai, Ziqiang Zhu, and Peisheng Xin, "Ka-band distributed MEMS phase shifters on silicon using AlSi suspended membrane," *Journal of Microelectromechanical Systems*, Vol, 13, No. 3, June 2004.
13. Rebeiz, G.M., Guan-Leng Tan, and Hayden, J.S., "RF MEMS Phase Shifter: Design and Applications," *IEEE Microwave Magazine*, Volume 3, Issue 2, pp72-81, June 2002.
14. Rainee N. Simons, "*Coplanar Waveguide Circuits, Components, and Systems*," John Wiley & Sons, Inc., 2001.
15. David M. Pozar, "Microwave Engineering," John Wiley & Sons, Inc., 1998.
16. M. J. W. Rodwell, S. T. Allen, R. Y. Yu, M. G. Case, U. Bhat tacharya, M. Reddy, E. Carman, M. Kamegawa, Y. Konishi, J. Pust, and R. Pallela, "Active and nonlinear wave propagation devices in ultrafast electronics and optoelectronics," *Proceedings of the IEEE*, vol. 82, no. 7, pp. 1037-1059, July 1994.
17. Janusz Grzyb and Gerhard Tröster, "Characteristic impedance deembedding of printed lines with probe-tip calibrations," *Proc. 32nd European Microwave Conference*, Milan, Italy, September 23-26, 2002.